1-1-1997

Site-selective excitation and polarized absorption and emission spectra of trivalent thulium and erbium in strontium fluorapatite

John B. Gruber

Andrew O. Wright

Michael D. Seltzer

Bahram Zandi

Larry D. Merkle

See next page for additional authors

Site-selective excitation and polarized absorption and emission spectra of trivalent thulium and erbium in strontium fluorapatite

Cite as: Journal of Applied Physics **81**, 6585 (1997); https://doi.org/10.1063/1.365197
Submitted: 09 October 1996 . Accepted: 04 February 1997 . Published Online: 17 August 1998

John B. Gruber, Andrew O. Wright, Michael D. Seltzer, Bahram Zandi, Larry D. Merkle, J. Andrew Hutchinson, Clyde A. Morrison, Toomas H. Allik, and Bruce H. T. Chai

Site-selective excitation and polarized absorption and emission spectra of trivalent thulium and erbium in strontium fluorapatite

John B. Gruber
Department of Physics, San José State University, San José, California 95192-0106

Andrew O. Wright and Michael D. Seltzer
Research and Technology Division, Naval Air Warfare Center, Code 474230D, China Lake, California 93555-6001

Bahram Zandi and Larry D. Merkle
IR Optics Technology OFC, Army Research Laboratory, Ft. Belvoir, Virginia 22060-5838

J. Andrew Hutchinson
Night Vision and Electronics Sensors Directorate, The United States Army, Ft. Belvoir, Virginia 22060-5806

Clyde A. Morrison
Army Research Laboratory, Adelphi, Maryland 20783-1145

Toomas H. Allik
Science Applications International Corporation, 1710 Goodridge Drive, McLean, Virginia 22102

Bruce H. T. Chai
Center for Research on Electro-optics and Lasers, University of Central Florida, Orlando, Florida 32836

(Received 9 October 1996; accepted for publication 4 February 1997)

Polarized fluorescence spectra produced by site-selective excitation, and conventional polarized absorption spectra were obtained for Tm^{3+} and Er^{3+} ions individually incorporated into single crystals of strontium fluorapatite, $Sr_5(PO_4)_3F$, also known as SFAP. Substitution of the trivalent rare earth ion for divalent strontium was achieved by passive charge compensation during Czochralski growth of the fluorapatite crystals. Spectra were obtained between 1780 and 345 nm at temperatures from 4 K to room temperature on crystals having the hexagonal structure $[P6_3/m(C_{6h}^2)]$. The polarized fluorescence spectra due to transitions from multiplet manifolds of $Tm^{3+}(4f^{12})$, including $^1D_2$, $^1G_4$, and $^3H_4$ to manifolds $^3H_6$ (the ground-state manifold), $^3F_4$, $^3H_5$, $^3H_4$, and $^3F_3$ were analyzed for the details of the crystal-field splitting of the manifolds. Fluorescence lifetimes were measured for Tm^{3+} transitions from $^1D_2$, $^1G_4$, and $^3H_4$ at room temperature and from $^1G_4$ at 16 K. Results of the analysis indicate that the majority of Tm^{3+} ions occupy sites having C_s symmetry. A point-charge lattice-sum calculation was made in which the crystal-field components, A_{nm}, were determined assuming that trivalent thulium replaces divalent strontium in the metal site having C_s symmetry. Results support the conclusion that the nearest-neighbor fluoride (F^-) is replaced by divalent oxygen (O^{2-}), thus preserving overall charge neutrality and local symmetry. Crystal-field splitting calculations predict energy levels in agreement with results obtained from an analysis of the experimental data. By varying the crystal-field parameters, B_{nm}, we obtained a rms difference of 7 cm^{-1} between 43 calculated and experimental Stark levels for $Tm^{3+}(4f^{12})$ in Tm:SFAP. Absorption and fluorescence spectra are also reported for Er^{3+} ions in Er:SFAP. Measurement of the temporal decay of the room temperature fluorescence from the $^4I_{11/2}$ and $^4I_{13/2}$ manifolds yielded fluorescence lifetimes of 230 ± 20 μs and 8.9 ± 0.1 ms, respectively. The experimental Stark levels obtained from an analysis of the spectroscopic data were compared with a crystal-field splitting calculation. The initial set of B_{nm} parameters for $Er^{3+}(4f^{11})$ was established from the three-parameter theory and the final set of B_{nm} parameters obtained for $Tm^{3+}(4f^{12})$ in Tm:SFAP. The best overall agreement between calculated and experimental Stark levels is 8 cm^{-1} for 48 Stark levels, representing 12 observed multiplet manifolds of $Er^{3+}(4f^{11})$ in Er:SFAP. [S0021-8979(97)01110-9]

I. INTRODUCTION

As a crystalline host for trivalent rare earth ions (R^{3+}), strontium fluorapatite $[Sr_5(PO_4)_3F]$, known as SFAP, has received growing attention as a laser host material or as a host for saturable Q-switch absorbers.[1–3] An expanding number of applications point to its excellent spectroscopic and physical properties.[4–6] This interest has been encouraged both by the size and optical quality of the crystals grown in recent years and by the development of diode pumping technology. A recent symposium on novel laser materials included a discussion on the advanced technology and applications for fluorapatites as host materials.[7]

In recent years details of the crystal-field splitting of energy levels of R^{3+} dopants such as Pr^{3+}, Nd^{3+}, Eu^{3+}, and

TABLE I. Absorption spectrum of Tm^{3+} in $Sr_5(PO_4)_3F$ at 4 K.[a]

$^{2S+1}L_J$[b]	λ (Å)[c]	α[d]	$E(cm^{-1})_{obs}$[e]	$E(cm^{-1})_{calc}$[f]	Γ_n^{calc}[g]	Percent free-ion mixture[h]					
$^3F_4$	17 729	0.20	5639[i*]	5646	2	99.3	$^3F_4$	+0.41	$^3H_6$	+0.14	$^3H_5$
	17 610	0.40	5677[i*]	5719	1	98.9	$^3F_4$	+0.50	$^3H_5$	+0.47	$^3H_6$
(6000)	17 487	0.05	5717								
	16 963	0.10	5894								
	16 915	0.38	5910[i*]	5909	1	98.1	$^3F_4$	+1.19	$^3H_5$	+0.54	$^3H_6$
	16 828	0.05	5941	5918	2	96.8	$^3F_4$	+2.78	$^3H_5$	+0.23	$^3H_6$
	16 765	0.04	5963[i*]	5970	1	98.7	$^3F_4$	+0.98	$^3H_5$	+0.16	$^3H_4$
	16 732	0.11	5975[i*]	5976	2	97.5	$^3F_4$	+1.81	$^3H_5$	+0.54	$^3H_6$
	16 256	0.16	6150[i*]	6137	1	98.3	$^3F_4$	+0.86	$^3H_6$	+0.62	$^3H_5$
	16 128	0.80	6199[i*]	6205	2	98.0	$^3F_4$	+1.05	$^3H_5$	+0.75	$^3H_6$
	16 065	0.05	6223								
	15 991	0.60	6252[i*]	6245	1	97.6	$^3F_4$	+1.91	$^3H_5$	+0.22	$^3H_4$
$^3H_5$	12 175	0.62	8211[i*]	8207	2	99.2	$^3H_5$	+0.45	$^3F_3$	+0.16	$^3F_4$
	12 170	0.30	8213[i*]	8215	1	99.2	$^3H_5$	+0.48	$^3F_3$	+0.15	$^3F_4$
(8647)	12 044(b)	0.17	8301*	8303	1	98.5	$^3H_5$	+0.86	$^3F_4$	+0.38	$^3F_3$
	12 025(sh)	0.10	8314								
	11 970	0.03	8352[i*]	8352	2	99.0	$^3H_5$	+0.54	$^3F_3$	+0.34	$^3F_4$
	11 886	0.03	8410[i*]	8405	2	99.2	$^3H_5$	+0.25	$^3F_3$	+0.21	$^3F_4$
	11 851	0.05	8436[i*]	8441	1	98.6	$^3H_5$	+0.67	$^3F_4$	+0.43	$^3F_3$
	11 810	0.02	8465*								
	11 651	0.01	8581								
	11 451	0.02	8730[i*]	8731	2	96.0	$^3H_5$	+3.48	$^3F_4$	+0.19	$^3H_4$
	11 270(b)	0.01	8870	8868	1	97.5	$^3H_5$	+1.66	$^3F_4$	+0.30	$^3F_2$
	11 170(b)	0.01	8950	8945	1	97.6	$^3H_5$	+1.69	$^3F_4$	+0.39	$^3H_4$
	10 715(b)	0.01	9330	9321	2	98.8	$^3H_5$	+0.52	$^3F_4$	+0.40	$^3F_2$
				9339	2	98.5	$^3H_5$	+0.89	$^3F_4$	+0.25	$^3F_2$
$^3H_4$	7943.2	4.25	12 586[i*]	12 586	2	97.8	$^3H_4$	+0.89	$^3F_3$	+0.87	$^3F_2$
	7937.5	3.64	12 595[i*]	12 595	1	99.0	$^3H_4$	+0.58	$^3F_3$	+0.18	$^3F_2$
(12 910)	7922.8	0.23	12 618								
	7913.3	3.18	12 633[i*]	12 635	1	98.0	$^3H_4$	+1.47	$^3F_3$	+0.18	$^3F_2$
	7893.9	0.15	12 665								
	7880.8	1.18	12 686[i*]	12 681	2	98.7	$^3H_4$	+0.94	$^3F_3$	+0.23	$^3H_5$
	7857.9	0.76	12 723[i]	12 726	1	97.8	$^3H_4$	+1.52	$^3F_2$	+0.27	$^3H_5$
	7848(sh)	0.06	12 740	12 740	2	97.1	$^3H_4$	+1.68	$^3F_2$	+0.81	$^3F_3$
	7809(b)	.02	12 802								
	7753.9	.01	12 893								
	7553(b)	0.05	13 236	13 230	2	96.0	$^3H_4$	+3.22	$^3F_3$	+0.27	$^3F_2$
	7525(sh)	0.08	13 285	13 266	1	95.0	$^3H_4$	+4.21	$^3F_3$	+0.23	$^3F_2$
	7519.1	0.26	13 296	13 320	1	94.0	$^3H_4$	+4.44	$^3F_3$	+0.98	$^3F_2$
$^3F_3$	6958.3	0.07	14 367*								
	6939.2	1.33	14 407[i*]	14 397	2	98.5	$^3F_3$	+1.13	$^3H_4$	+0.13	$^3H_5$
(14 675)	6918.0	0.05	14 451								
	6811.2	0.42	14 677[i*]	14 668	1	97.5	$^3F_3$	+1.42	$^3H_4$	+0.39	$^3F_2$
	6807.4	0.32	14 688[i*]	14 693	2	96.9	$^3F_3$	+2.39	$^3H_4$	+0.37	$^3F_2$
	6769.0	0.04	14 769	14 775	1	93.0	$^3F_3$	+5.67	$^3H_4$	+0.48	$^3F_2$
	6752.9	0.42	14 804[i*]	14 816	2	97.1	$^3F_3$	+1.68	$^3H_4$	+0.60	$^3H_5$
	6731.1	0.48	14 852[i*]	14 859	1	93.6	$^3F_3$	+3.02	$^3H_4$	+2.48	$^3F_2$
	6717.2	0.08	14 883[i*]	14 879	2	98.3	$^3F_3$	+0.59	$^3H_5$	+0.52	$^3H_4$
$^3F_2$	6405.8	0.03	15 607[i]	15 600	1	95.9	$^3F_2$	+2.05	$^3F_3$	+1.65	$^3H_4$

TABLE I. *(Continued.)*

$^{2S+1}L_J$[b]	λ (Å)[c]	α[d]	$E(cm^{-1})_{obs}$[e]	$E(cm^{-1})_{calc}$[f]	Γ_n^{calc}[g]	Percent free-ion mixture[h]					
	6389.9	0.20	15 645[i]	15 652	1	99.0	$^3F_2$	+0.37	$^3H_4$	+0.26	$^3F_3$
(15 846)	6243(b)	0.01	16 014	16 024	2	97.1	$^3F_2$	+1.77	$^3H_4$	+0.63	$^3F_3$
	6206(sh)	0.01	16 109	16 110	1	97.4	$^3F_2$	+1.64	$^3H_4$	+0.46	$^3F_3$
	6199(b)	0.01	16 127	16 132	2	97.5	$^3F_2$	+1.22	$^3H_4$	+0.60	$^3F_3$
$^1G_4$	4757.0	0.13	21 016[i]	21 017	2	99.5	$^1G_4$	+0.19	$^3H_4$	+0.12	$^3F_3$
	4742.5	0.30	21 081[i]	21 083	1	99.6	$^1G_4$	+0.12	$^1I_6$	+0.10	$^3F_3$
	4735.4	0.02	21 112								
(21 459)	4733.0	0.03	21 122								
	4711.2	0.13	21 221[i]	21 214	2	99.6	$^1G_4$	+0.13	$^1D_2$	+0.09	$^1I_6$
	4709.0	0.18	21 230[i]	21 231	1	99.5	$^1G_4$	+0.21	$^1D_2$	+0.08	$^3P_2$
	4703.2	0.03	21 256								
	4699.2	0.02	21 274								
	4664.4	0.10	21 433								
	4656.8	0.38	21 468[i]	21 472	1	99.5	$^1G_4$	+0.15	$^1I_6$	+0.13	$^1D_2$
	4647.5	0.26	21 511	21 477	2	99.5	$^1G_4$	+0.15	$^1I_6$	+0.15	$^1D_2$
	4639.0	0.02	21 550								
				21 680	2	99.6	$^1G_4$	+0.14	$^1D_2$	+0.09	$^3H_5$
	4577(b)	0.01	21 842	21 827	1	99.6	$^1G_4$	+0.17	$^3F_3$	+0.14	$^3H_4$
	4532(b)	0.01	22 060	22 069	1	99.7	$^1G_4$	+0.08	$^3H_4$	+0.05	$^3P_2$
$^1D_2$	3657.9	0.44	27 330[i]	27 330	1	99.7	$^1D_2$	+0.09	$^3F_3$	+0.07	$^1G_4$
(27 607)											

[a]Crystal contains 0.12 at. % Tm ($1.4\times10^{19}/cm^3$).
[b]Multiplet manifolds of Tm^{3+} ($4f^{12}$); calculated centroids are listed in parenthesis in cm^{-1}.
[c]Wavelength (angstroms); b denotes broad; sh denotes shoulder.
[d]Intensity of axial spectrum at 4 K in absorbance/cm.
[e]Energy level observed in absorption (cm^{-1}); levels also observed in fluorescence are marked with a star (*).
[f]Calculated energy level based on Tm^{3+} ions occupying M(II) sites having C_s symmetry using crystal-field parameters (B_{nm}) reported in Table VI.
[g]Predicted symmetry label (Γ_n) of calculated Stark level.
[h]Percent free-ion mixture of wave functions based on C_s symmetry crystal-field parameters (B_{nm}) reported in Table VI.
[i]Energy levels used in final fitting analysis.

Er^{3+} in either SFAP or its analogue $Ca_5(PO_4)_3F$, known as FAP, have become better understood through analyses of site-selective excitation and emission spectroscopy.[1,4,8–11] In Pr:SFAP[4] as well as in Eu:SFAP,[8] a single predominant site was determined spectroscopically; however, crystal-field splitting calculations did not yield satisfactory agreement with experimental Stark levels in either case. Similar calculations were more successful in analyzing the spectra of Nd^{3+} and Er^{3+} ions in Nd:SFAP, Nd:FAP, and Er:FAP.[1,11] In the present study we chose Tm^{3+} as an optical probe in order to gain more specific information regarding the charge-compensated site occupied by the majority of R^{3+} ions in SFAP.[12–19] The energy levels of Tm^{3+} are associated with a relatively simple electronic configuration ($4f^{12}$) with a sufficient number of multiplet manifolds, $^{2S+1}L_J$, separated by a large spin-orbit splitting to permit a detailed analysis of the crystal-field splitting of the isolated manifolds.

In the present study we find that site-selective polarized emission spectra representing transitions from $^1D_2$, $^1G_4$, and $^3H_4$ to manifolds $^3H_6$, $^3F_4$, $^3H_5$, $^3H_4$ and $^3F_3$ of Tm^{3+} in Tm:SFAP are consistent with electric-dipole selection rules for C_s symmetry. We find agreement between the observed Stark levels and the symmetry labels established for many of these levels obtained from an analysis of the polarized fluorescence data, and the calculated Stark levels and predicted symmetry labels based on a crystal-field splitting calculation in which the crystal-field Hamiltonian has C_s symmetry. The starting set of crystal-field components, A_{nm}, were derived from a lattice-sum calculation in which the F^- ion, which is nearest-neighbor ion to the M(II) site in which Tm^{3+} resides, is replaced by O^{2-} so that charge neutrality is maintained throughout the lattice.[18] By varying the initial set of crystal-field parameters, B_{nm}, in order to optimize agreement between the calculated and observed Stark levels, we obtained a final rms value of 7 cm^{-1} between the energies of 43 calculated and observed Stark levels. There is consistent agreement between the calculated and the experimentally assigned symmetry labels for these Stark levels as well.

From the final set of B_{nm} parameters for Tm^{3+} we derived a starting set of parameters to be used in the crystal-field splitting analyses of the multiplet manifolds of $Er^{3+}(4f^{11})$ ions in Er:SFAP. In C_s symmetry all Stark levels of Kramers ions such as Er^{3+} (having an odd number of electrons in the electronic configuration) are twofold degenerate and have the same symmetry label, ($^2\Gamma_6$). Both electric- and magnetic-dipole transitions are allowed between these Stark levels.[1] With a small change in B_{nm}, parameters resulting from a least-squares fitting procedure, we obtained a rms difference of 8 cm^{-1} for 48 Stark levels of Er^{3+} in Er:SFAP assuming the Er^{3+} ions reside in sites of C_s symmetry. The results of the present study support the earlier conclusion of Wright *et al.*[4,8] that the majority of

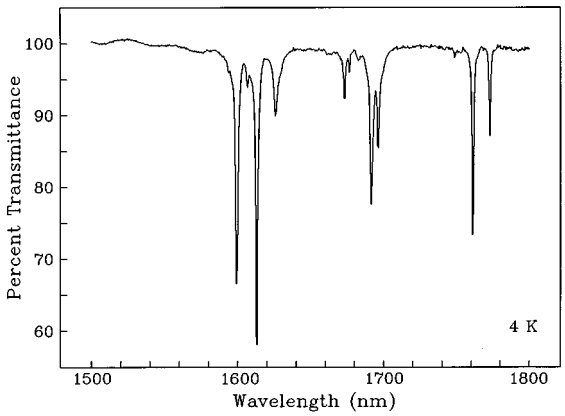

FIG. 1. Axial absorption spectrum of $^3F_4$, Tm^{3+} in Tm:SFAP (4 K).

R^{3+} ions occupy sites of C_s symmetry in the SFAP lattice and also support the assumption that in SFAP the nearest neighbor (F^-) to the metal site M(II) having C_s symmetry in the undoped crystal is replaced by divalent oxygen (O^-), thus preserving charge neutrality when the R^{3+} ion replaces the Sr^{2+} ion in the M(II) site.

II. EXPERIMENTAL DETAILS

Crystals of $Sr_5(PO_4)_3F$ containing either Tm^{3+} ions or Er^{3+} ions were grown by the Czochralski method at the University of Central Florida, Center for Research on Electro-optics and Lasers.[7] The amount of rare earth in each sample used in our studies was determined by Galbraith Laboratories (Knoxville, TN), the results of which agree with determinations using inductively coupled plasma atomic emission spectrometry on chemically digested portions of the crystals. The data appearing in Tables I–III for Tm^{3+} in Tm:SFAP, and in Tables IV and V for Er^{3+} in Er:SFAP represent concentrations of 0.12 at. % Tm and 0.15 at. % Er, respectively.

Data appearing in Tables I–V are based on single crystals having a hexagonal structure [space group $P6_3/m(C_{6h}^2)$].[20] There are two molecules per unit cell.[21,22] In the undoped crystal 40% of the Sr^{2+} ions occupy the M(I) site (C_3 symmetry), and the remaining 60% occupy the M(II) site (C_s symmetry). We observed no spectroscopic evidence to suggest a phase change in the crystals below room temperature.[23,24]

The crystals were cut and polished parallel and perpendicular to the optical or c-axis. Axial and polarized transverse spectra (σ and π polarizations) were obtained after the optical axis was determined by placing the crystal between crossed polarizers to observe the characteristic maltese cross pattern.[8] Absorption spectra were obtained using a Cary model 2390 spectrophotometer equipped with a continuous-flow liquid-helium cryostat (Oxford, Model 1204D) that allowed us to obtain spectra at any temperature between 4 K and room temperature. The instrument was calibrated by measuring deuterium emission lines in different orders. Supplemental absorption spectra were obtained at a temperature of approximately 35 K from a Perkin–Elmer Lambda 9 spectrophotometer equipped with a closed-cycle helium refrigerator.

Site-selective excitation and fluorescence spectra were obtained at 4 K using a Quantel Nd:YAG laser-pumped dye laser with an output bandwidth of about 0.1 cm^{-1}. A 0.85 m double monochromator was used for fluorescence detection. Signals were processed using a boxcar averager and gated integrator. Data were collected and stored in a digital oscilloscope. Fluorescence lifetime measurements on Tm^{3+} samples were taken using a Continuum Nd:YAG Q-switched laser and relatively broad-band dye laser with Rhodamine dyes. We did not attempt to carry out site-selective lifetimes studies with this instrumentation. The frequency-tripled Nd:YAG output was used to excite $^1D_2$ whereas the dye laser output excited $^1G_4$ (via anti-Stokes Raman shifting in H_2 gas) and $^3H_4$ (via Stokes Raman shifting). Detection was accomplished using a Spex monochromator, a Hamamatsu photomultiplier, and a Tektronix digitizing oscilloscope.

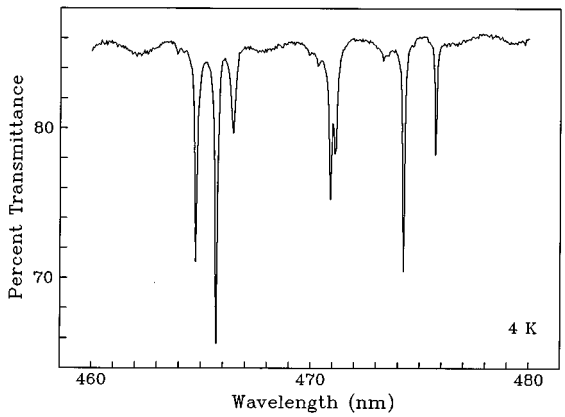

FIG. 2. Axial absorption spectrum of $^1G_4$, Tm^{3+} in Tm:SFAP (4 K).

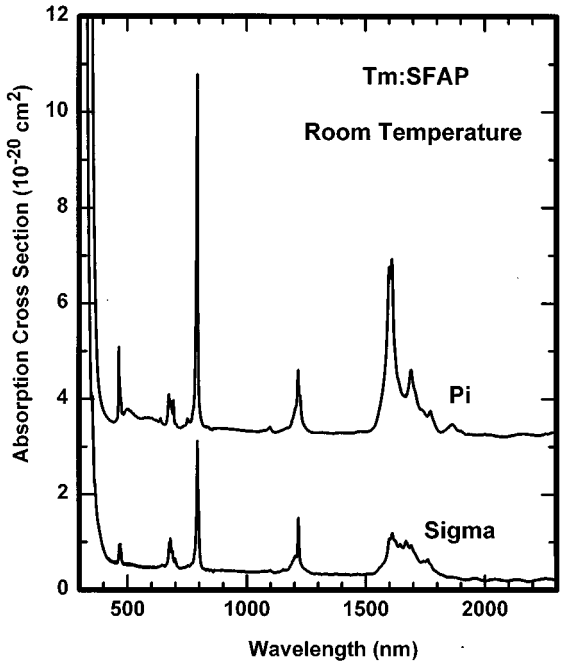

FIG. 3. Room temperature polarized absorption spectra of Tm:SFAP.

TABLE II. Emission from $^1G_4$ to $^3H_6$, $^3F_4$, and $^3H_5$:Tm^{3+} in $Sr_5(PO_4)_3F$ at 4 K.[a]

λ(Å)[b]	I[c]	P[d]	E(cm^{-1})[e]	ΔE[f] (cm^{-1})	Γ_n[g]	E(cm^{-1})[h] (obs.)	E(cm^{-1})[i] (calc.)	Γ_n[j] (calc.)	$^{2S+1}L_J$[k]
4757.8	vs	σ	21 012	0	2	0	2	2	
4758.8	vs	π	21 008	4	1	4	4	1	
4773.8	m	σ	20 942	70	2	70	68	2	$^3H_6$
4779(sh)	w	π	20 919	93	1	90	86	1	
4799.7	m	π	20 829	183	1	175(b)	174	1	(549)
4796.3	m	σ	20 844	168	2		190	2	
4822(b)	m	π	20 732						
4842.5	vw	π	20 645						
							504	2	
							511	1	
4923.5	m	π	20 305	707[l]	1		673	1	
							881	2	
							950	2	
							1300	1	
5078.1	w	π	19 687	1325	1		1319	1	
6502.2	s	σ	15 375	5637	2	5639	5646	2	
6518.1	vs	π	15 338	5674	1	5678	5719	1	$^3F_4$
						5717			
6618.8	m	π	15 104	5908	1	5910	5909	1	(6000)
6620(sh)	m		15 100	5912		5914	5918	2	
6642.2	s	π	15 051	5961	1	5963	5970	1	
6647.4	m	σ	15 039	5973	2	5975	5976	2	
6725.4	m	π	14 865	6147	1	6150	6137	1	
6747.9	m	σ	14 815	6197	2	6199	6205	2	
6771.6	w	π	14 763	6249	1	6252	6245	1	
7808.5	vs	σ	12 803	8209	2	8211	8207	2	
7808(sh)	s	π	12 800	8212	1	8213	8215	1	
7866(vb)	m	π	12 709	8303	1	8301(vb)	8303	1	$^3H_5$
7871(vb)	m	π	12 701	8311[l]	1				
7895.4	w	σ	12 662	8350	2	8352	8352	2	(8647)
7934(b)	m		12 604	8408		8410	8405	2	
7948.8	s	π	12 577	8435	1	8436	8441	1	
8137.3	s		12 286	8726		8730	8731	2	
						8870(b)	8868	1	
						8950(b)	8945	1	
							9321	2	
						9330(b)	9339	2	

[a]Crystal contains 0.12 at. % Tm (1.4×10^{19}/cm^3).
[b]Emission observed from lowest Stark level of $^1G_4$ identified in absorption (Table I) at 4757.0 A; sh (shoulder), b (broad), vb (very broad).
[c]Relative intensity (axial spectrum) within a multiplet manifold, vs (very strong), s (strong), m (medium), w (weak), vw (very weak).
[d]Polarization of the transverse emission spectra (4 K).
[e]Energy of the transition in cm^{-1}.
[f]Energy difference based on emitting level at 21 012 cm^{-1}.
[g]Assigned symmetry label on the assumption of C_s symmetry selection rules for Tm^{3+} ions occupying M(II) sites.
[h]Stark levels 70, 90, and 175 cm^{-1} are based on analysis of absorption hot bands; other levels were identified from absorption spectra obtained ~4 K.
[i]Calculated splitting based on crystal-field parameters (B_{nm}) reported in Table VI.
[j]Symmetry label of calculated Stark level obtained using B_{nm} parameters reported in Table VI.
[k]Multiplet manifold of Tm^{3+} ($4f^{12}$); number in parenthesis is the calculated centroid.
[l]Levels not included in the final fitting analysis.

Temperature dependent data were acquired using a CTI closed cycle refrigerator system.

Room temperature fluorescence lifetime measurements on Er^{3+} samples were taken using a temperature-tuned, pulsed, Spectra Diode Labs InGaAs laser diode array with the fluorescence being detected with a Germanium Power Devices Ge photodiode. Wavelength selection was accomplished with colored glass filters.

III. THE OBSERVED SPECTRA OF Tm:SFAP

We report the axial absorption spectrum of Tm:SFAP (4 K) in Table I (column 2) between 1780 and 345 nm. This

TABLE III. Emission from $^1D_2$ to $^3H_6$, $^3F_4$, $^3H_5$, and $^3F_3$:Tm^{3+} in $Sr_5(PO_4)_3F$ at 4 K.[a]

λ(Å)[b]	I[c]	P[d]	$E(cm^{-1})$[e]	ΔE[f] (cm^{-1})	Γ_n[g]	$E(cm^{-1})$[h] (obs.)	$E(cm^{-1})$[i] (calc.)	Γ_n[j] (calc.)	$^{2S+1}L_J$[k]
3648.8	vw		27 398						
3658.4	vs	π	27 327	0	2	0	2	2	$^3H_6$
3659(sh)	m	σ	27 322	4	1	4	4	1	(549)
3667.8	w		27 257	70		70	68	2	
3670(sh)	w	σ	27 237	90	1	90	86	1	
3680.4	vs	π	27 163	164	2	175(b)	174	1	
3683.2	s	σ	27 143	184	1		190	2	
3695.3(b)	w	σ	27 054	273[l]					
3697.6(b)	w	π	27 037	290[l]					
							504	2	
							511	1	
3755(b)	vw		26 624	705[j]			673	1	
							881	2	
							950	2	
3842(sh)	m	σ	26 021	1306[l]	1		1300	1	
3844.8	vs	σ	26 002	1325	1		1319	1	
4602.6	vw	π	21 721						
4610.0	vs	π	21 686	5641	2	5639	5646	2	$^3F_4$
4617.8	vs		21 649	5678		5677	5719	1	
4653.7	vw		21 482						(6000)
4664.6	m		21 432						
4667.9	vs	σ	21 417	5910	1	5910	5909	1	
4680.0	m	σ	21 362	5965	1	5963	5970	1	
4682.2	m	π	21 352	5975	2	5975	5976	2	
4689(sh)	vw		21 321						
4721.0	m		21 176	6151		6150	6137	1	
4732.2	m	π	21 126	6201	2	6199	6205	2	
4744.0	vw		21 073	6254		6252	6245	1	
5231(sh)	m	π	19 114	8213	2	8211	8207	2	$^3H_5$
5229.4	s	σ	19 117	8210	1	8213	8215	1	
5255(b)	m	σ	19 024	8303	1	8301	8303	1	(8647)
5261(sh)	vw		19 001						
5269.6	s	π	18 974	8353	2	8352	8352	2	
5272(sh)	vw		18 961						
5284(b)	s	π	18 920	8407	2	8410	8405	2	
5294.7	s		18 882	8445[l]		8436	8441	1	
5332(b)	w		18 749	8578[l]		8581			
5375(b)	m	π	18 599	8728	2	8730	8731	2	
5390(b)	vw		18 548						
						8870	8868	1	
						8950	8945	1	
						9330	9321	2	
							9339	2	
6761.9	vw		14 785						
6780.9	s	π	14 743	12584	2	12 586	12 586	2	$^3H_4$
6785.2	vs	σ	14 734	12593	1	12 595	12 595	1	
6803.0	vs	σ	14 695	12 632	1	12 633	12 635	1	(12 910)
6827.7	m	π	14 642	12 685	2	12 686	12 681	2	
						12 723	12 726	1	
						12 740[l]	12 740	2	
6880.8	m	π	14 529	12 798		12 802(vw)			
6891(vb)	w	π	14 491	12 836					
6925.5	m	π	14 435	12 892		12 893[l]			
						13 236[l]	13 230	2	
						13 285[l]	13 266	1	
						13 296	13 320	1	
7713.0	m	π	12 962						
7736.7	s	π	12 922	14 405	2	14 407	14 397	2	$^3F_3$
7902.4	s	σ	12 651	14 676	1	14 677	14 668	1	
7908.1	s		12 642	14 685		14 688	14 693	2	(14 675)
						14 769	14 775	1	
7981.8	m	π	12 525	14 802	2	14 804	14 816	2	
8014.0	m	σ	12 475	14 852	1	14 852	14 859	1	
8033.3	vs	π	12 445	14 882	2	14 883	14 879	2	

[a]Crystal contains 0.12 at. % Tm ($1.4\times10^{19}/cm^3$).
[b]Emission observed from lowest Stark level of $^1D_2$ identified in absorption (Table I) at 3657.9 Å; sh (shoulder), b (broad), vb (very broad).
[c]Relative intensity (axial spectrum) within a multiplet manifold, vs (very strong), s (strong), m (medium), w (weak), vw (very weak).
[d]Polarization of the transverse emission spectra (4 K).
[e]Energy of the transition in cm^{-1}.
[f]Energy difference based on emitting level at 27 327 cm^{-1}.
[g]Assigned symmetry label based on the assumption of C_s symmetry selection rules for Tm^{3+} ions occupying M(II) sites.
[h]Stark levels 70, 90, and 175 cm^{-1} based on analysis of absorption hot bands; other levels based on analysis of 4 K absorption spectrum.
[i]Calculated splitting based on B_{nm} parameters reported in Table VI.
[j]Symmetry label of calculated Stark level obtained using B_{nm} parameters in Table VI.
[k]Multiplet manifold of Tm^{3+} ($4f^{12}$); number in parenthesis is the calculated centroid.
[l]Levels not included in the final fitting analysis.

wavelength range includes the spectra of transitions to multiplet manifolds of Tm^{3+} ($4f^{12}$) including $^3F_4$, $^3H_5$, $^3H_4$, $^3F_3$, $^1G_4$, and $^1D_2$. At wavelengths shorter than 310 nm the crystal itself begins to absorb, making it impossible to observe spectra of the $^1I_6$ and ^3P_J manifolds. Only the lowest energy (emitting Stark level) of the $^1D_2$ manifold is reported since the onset of the absorption by the crystal also includes spectra possibly due to defects and centers attributed to the charge-compensation required to preserve charge neutrality in the lattice.[11]

The absorption spectrum of each manifold usually consists of $2J+1$ relatively strong peaks along with weaker and usually broader peaks which are attributed to Tm^{3+} ions in minority sites. Representative spectra obtained at 4 K are given in Fig. 1 ($^3F_4$) and Fig. 2 ($^1G_4$). A survey of the polarized absorption spectra of Tm:SFAP obtained at room temperature is given in Fig. 3. At room temperature the spectra are observed in both σ and π polarizations. At temperatures approaching 4 K the sharpest peaks have sufficient resolution to indicate that transitions occur from the ground-state Stark level and the first excited-state Stark level separated by only 4 cm^{-1}. The polarization of the 4 K absorption spectra of the sharpest peaks indicates that the ground-state Stark level and the 4 cm^{-1} excited state Stark level have different symmetries. The clearest evidence for these observations is found among the spectra of the $^3F_3$ multiplet manifold, although to varying degrees of resolution, the 4 K spectra of other multiplet manifolds show similar evidence for the 4 cm^{-1} splitting. In Fig. 4 for example the 4 and 10 K polarized absorption spectra are given for the emitting Stark level in $^1G_4$ (475.7 nm, Table I). The growth of hot bands observed at 10 K provides evidence for the 4 cm^{-1} splitting. However, we relied on site-selective excitation to produce polarized fluorescence to help us resolve the dilemma.

Polarized fluorescence spectra obtained by site-selective excitation were observed from the $^1D_2$ (366 nm), $^1G_4$ (476 nm), and $^3H_4$ (794 nm) levels to the ground-state manifold, $^3H_6$. The spectra clearly indicate that the ground-state Stark level and the first excited Stark level have different symmetry and are separated by 4 cm^{-1}. Table II presents the polarized fluorescence spectra from $^1G_4$ to $^3H_6$, $^3F_4$, and $^3H_5$, multiplet manifolds. Table III reports the polarized fluorescence spectra observed from $^1D_2$ to $^3H_6$, $^3F_4$, $^3H_5$, $^3H_4$, and $^3F_3$. The data in both tables were obtained at 4 K. The strongest $2J+1$ absorption peaks for manifolds also observed in fluorescence can be matched to Stark levels whose energy and symmetry are determined from an analysis of the polarized fluorescence appearing in Tables II and III. Figure 5 is a composite figure showing the sigma, pi, unpolarized transverse, and the axial spectra for transitions from $^1G_4$ to $^3H_6$. A similar composite represents fluorescence from $^1G_4$ to $^3F_4$ (Fig. 6), $^1G_4$ to $^3H_5$ (Fig. 7), and $^1D_2$ to $^3F_4$ (Fig. 8).

The polarized fluorescence spectra can be interpreted by assuming that the Tm^{3+} ions occupy sites of C_s symmetry. In such symmetry Stark levels are labeled either Γ_1 or Γ_2.[25] In the transverse spectrum both electric- and magnetic-dipole transitions have the same selection rules.[26]

C_s	Γ_1	Γ_2
Γ_1	σ	π
Γ_2	π	σ

Transitions appearing in both the transverse σ-polarized spectrum and the axial spectrum are electric-dipole in character and represent the only type of transition observed.

The polarizations reported in Tables II and III suggest that the emitting Stark levels from $^1G_4$ and $^1D_2$ have different symmetries since the terminal levels are the same. If we choose Γ_1, for the emitting $^1G_4$ level (Table II, 21 012 cm^{-1}) and Γ_2 symmetry for the emitting $^1D_2$ level (Table III, 27 327 cm^{-1}) based on the predicted symmetries obtained from calculations described in the next section, we find complete consistency both in energy and symmetry label for the most intense fluorescence peaks appearing in both tables. Symmetry label assignments (Γ_1 or Γ_2) have been made to all Stark levels where polarized transitions to that level are unambiguous. Since these assignments can be applied to nearly all the spectra reported in Tables II and III we conclude that the majority of Tm^{3+} ions occupy a site having C_s symmetry.

IV. FLUORESCENCE LIFETIME MEASUREMENTS ON Tm:SFAP

Fluorescence lifetime measurements can be useful in learning more regarding the interaction between the Tm^{3+} ions and the host lattice, SFAP. Decay waveforms have been measured for emission from multiplet manifolds $^1G_4$, $^1D_2$, and $^3H_4$ to the ground-state manifold, $^3H_6$. Figure 9 shows the room temperature fluorescence decay waveforms for $^1G_4$ and $^3H_4$. The $^1G_4$ emission exhibits a nearly exponential decay with only a very weak faster initial decay. This observation supports the assumption that the spectra are dominated by Tm^{3+} ions in a single type of site. The fact that the decay lifetime shows relatively little temperature dependence, changing from about 340 μs at 16 K to about 310 μs at room temperature, suggests that the lifetime may be predominantly radiative. This lifetime is somewhat shorter than the comparable emission observed for Tm^{3+} ions in some other host crystals such as Y_2SiO_5,[27] but is consistent with the strong transitions evident in the Tm:SFAP absorption data (see Fig. 3). The room temperature emission from the $^1D_2$ to the $^3H_6$ manifold exhibits a single exponential decay with a lifetime of 9.1 μs.

However, the $^3H_4$ room temperature emission monitored at 795 nm following excitation at 788 nm, exhibits very different behavior. This decay, also shown in Fig. 9, is well approximated by the sum of two exponentials, with lifetimes of 3.0 and 37 μs. These results indicate that emitting Tm^{3+} ions occupy at least two different environments. The brevity of these lifetimes, compared to the $^3H_4$ lifetime in other hosts, suggests that nonradiative processes are important at least for the faster decay.[27–29] About two-thirds of the integrated intensity is in the faster decay, despite the likelihood that strong quenching gives it a low probability per ion of fluorescing. There is evidence of minority site absorption to $^3H_4$, particularly in the shoulders of the intense absorption peaks at 7943.2 and 7937.5 Å (Table I). However, time resolved spectroscopy did not reveal distinct fluorescence

TABLE IV. Absorption spectrum of Er^{3+} in $Sr_5(PO_4)_3F$ at 4 K.[a]

$^{2S+1}L_J$[b]	λ (Å)[c]	α[d]	$E(cm^{-1})_{obs}$[e]	$E(cm^{-1})_{calc}$[f]	Percent free-ion mixture[g]					
$^4I_{13/2}$	15 336	0.01	6519							
	15 306	0.73	6532[h,i]	6542	99.8	$^4I_{13/2}$	+0.06	$^4I_{11/2}$	+0.04	$^4G_{9/2}$
(6715)	15 172	0.22	6589[h,i]	6583	99.8	$^4I_{13/2}$	+0.09	$^4I_{11/2}$	+0.04	$^4I_{15/2}$
	15 163(sh)	0.15	6592							
	15 124	0.51	6610[h,i]	6615	99.8	$^4I_{13/2}$	+0.09	$^4I_{11/2}$	+0.06	$^4I_{15/2}$
	15 095(b)	0.02	6624							
	15 052	0.15	6643[h,i]	6635	99.8	$^4I_{13/2}$	+0.09	$^4I_{11/2}$	+0.04	$^4I_{15/2}$
	15 020(b)	0.01	6656							
	14 940(b)	0.05	6690[i]	6690	99.7	$^4I_{13/2}$	+0.22	$^4I_{11/2}$	+0.04	$^4I_{15/2}$
	14 680(b)	0.02	6810[i]	6807	99.5	$^4I_{13/2}$	+0.34	$^4I_{11/2}$	+0.06	$^4I_{15/2}$
	14 210	0.12	7035[h,i]	7036	99.8	$^4I_{13/2}$	+0.13	$^4I_{11/2}$	+0.04	$^4I_{15/2}$
$^4I_{11/2}$	9815.0	0.01	10 186							
	9797.2	0.17	10 204[h,i]	10 203	99.7	$^4I_{11/2}$	+0.13	$^4I_{13/2}$	+0.08	$^4I_{9/2}$
(10 304)	9771.1	0.06	10 225[i]	10 219	99.6	$^4I_{11/2}$	+0.15	$^4I_{9/2}$	+0.10	$^4I_{13/2}$
	9765.0	0.04	10 238[i]	10 244	99.7	$^4I_{11/2}$	+0.09	$^4I_{13/2}$	+0.07	$^4F_{9/2}$
	9750.1	0.03	10 253[i]	10 255	99.6	$^4I_{11/2}$	+0.17	$^4F_{9/2}$	+0.17	$^4I_{13/2}$
	9704(b)	0.01	10 302							
	9659(b)	0.01	10 350[i]	10 349	99.5	$^4I_{11/2}$	+0.27	$^4I_{13/2}$	+0.15	$^4F_{9/2}$
	9540(b)	0.04	10 480	10 503	99.5	$^4I_{11/2}$	+0.26	$^4I_{13/2}$	+0.10	$^4I_{9/2}$
$^4I_{9/2}$	8087.0	0.08	12 362[h,i]	12 373	99.7	$^4I_{9/2}$	+0.10	$^2H_{11/2}$	+0.10	$^4F_{9/2}$
	8014.0	0.02	12 475[i]	12 469	99.3	$^4I_{9/2}$	+0.30	$^4F_{9/2}$	+0.18	$^4I_{11/2}$
(12 549)	7977.5	0.16	12 533[i]	12 529	99.5	$^4I_{9/2}$	+0.27	$^4F_{9/2}$	+0.09	$^4I_{11/2}$
	7948.0	0.09	12 578[i]	12 580	99.5	$^4I_{9/2}$	+0.14	$^4F_{9/2}$	+0.10	$^4I_{11/2}$
	7863(b)	0.02	12 714[i]	12 710	99.2	$^4I_{9/2}$	+0.58	$^4F_{9/2}$	+0.09	$^2H_{11/2}$
$^4F_{9/2}$	6619.5	0.25	15 103[h,i]	15 120	98.3	$^4F_{9/2}$	+0.86	$^4I_{9/2}$	+0.46	$^2H_{11/2}$
	6614.5	0.01	15 114							
(15 304)	6611.1	0.01	15 122							
	6601.0	0.44	15 145[h,i]	15 140	99.1	$^4F_{9/2}$	+0.48	$^2H_{11/2}$	+0.16	$^4I_{9/2}$
	6594.6	0.02	15 160							
	6566(b)	0.16	15 226							
	6564(sh)	0.10	15 230							
	6540(b)	0.03	15 286	15 285	99.3	$^4F_{9/2}$	+0.32	$^2H_{11/2}$	+0.11	$^4I_{9/2}$
	6481.2	0.21	15 425[h,i]	15 412	99.5	$^4F_{9/2}$	+0.15	$^4I_{9/2}$	+0.13	$^2H_{11/2}$
	6427.5	0.27	15 552[h]	15 517	99.6	$^4F_{9/2}$	+0.17	$^4I_{9/2}$	+0.08	$^4I_{11/2}$
$^4S_{3/2}$	5492.1	0.19	18 203[h,i]	18 208	97.6	$^4S_{3/2}$	+2.12	$^2H_{11/2}$	+0.07	$^4I_{9/2}$
	5487.2	0.02	18 219							
(18 346)	5477.0	0.02	18 253							
	5429.2	0.08	18 414[h,i]	18 408	94.0	$^4S_{3/2}$	+5.69	$^2H_{11/2}$	+0.09	$^4F_{7/2}$
	5420.4	0.01	18 444							
$^2H_{11/2}$	5281.0	0.02	18 931							
	5272.9	1.19	18 960[h]	19 043	98.3	$^2H_{11/2}$	+0.73	$^4F_{7/2}$	+0.67	$^4S_{3/2}$
(19 149)	5267.4	0.04	18 979							
	5232.3	0.02	19 107							
	5231.1	0.02	19 111[i]	19 105	98.4	$^2H_{11/2}$	+0.76	$^4S_{3/2}$	+0.58	$^4F_{7/2}$
	5226.2	0.03	19 129							
	5221.8	3.33	19 145[h,i]	19 136	96.8	$^2H_{11/2}$	+1.62	$^4F_{7/2}$	+1.26	$^4S_{3/2}$
	5215.7	2.09	19 168[h,i]	19 174	94.6	$^2H_{11/2}$	+3.97	$^4S_{3/2}$	+0.88	$^4F_{7/2}$
	5213.6(sh)	0.20	19 175							
	5210.9	0.04	19 188							
	5202(sh)	1.30	19 218							
	5199.8	3.25	19 226[h,i]	19 234	97.6	$^2H_{11/2}$	+0.96	$^4F_{7/2}$	+0.59	$^4S_{3/2}$
	5191.8	3.30	19 256[h,i]	19 252	97.5	$^2H_{11/2}$	+1.16	$^4F_{7/2}$	+0.64	$^4S_{3/2}$
	5189(sh)	0.40	19 266							
	5183.0	0.05	19 288							
$^4F_{7/2}$	4951.0	0.01	20 192							
	4948.8	0.04	20 201							
(20 505)	4945.4	0.83	20 215[h,i]	20 213	97.6	$^4F_{7/2}$	+1.47	$^2H_{11/2}$	+0.36	$^4G_{9/2}$

TABLE IV. *(Continued.)*

$^{2S+1}L_J$[b]	λ (Å)[c]	α[d]	$E(cm^{-1})_{obs}$[e]	$E(cm^{-1})_{calc}$[f]	Percent free-ion mixture[g]					
	4941(b)	0.03	20 233							
	4936.2	0.01	20 253							
	4878.0	0.17	20 494[h,i]	20 490	96.4	$^4F_{7/2}$	+2.13	$^2H_{11/2}$	+0.66	$^4F_{5/2}$
	4875.2	0.02	20 506							
	4855.5	0.13	20 589[h,i]	20 589	96.4	$^4F_{7/2}$	+1.51	$^4F_{5/2}$	+1.50	$^2H_{11/2}$
	4854(sh)	0.03	20 596							
	4838.3	0.49	20 663[h,i]	20 667	97.8	$^4F_{7/2}$	+1.04	$^2H_{11/2}$	+0.66	$^4F_{5/2}$
	4836(sh)	0.07	20 672							
$^4F_{5/2}$	4537.6	0.17	22 032[h,i]	22 013	97.7	$^4F_{5/2}$	+0.91	$^4F_{7/2}$	+0.53	$^4F_{3/2}$
	4536(sh)	0.03	22 040							
(22 112)	4533.1	0.01	22 054							
	4532.2	0.07	22 058[i]	22 053	73.7	$^4F_{5/2}$	+24.2	$^4F_{3/2}$	+1.23	$^4F_{7/2}$
	4522.0	0.12	22 108[h,i]	22 130	92.2	$^4F_{5/2}$	+6.52	$^4F_{3/2}$	+0.89	$^4F_{7/2}$
	4520(sh)	0.02	22 118							
$^4F_{3/2}$	4453(b)	0.01	22 452							
	4450.0	0.02	22 466[i]	22 475	75.1	$^4F_{3/2}$	+24.1	$^4F_{5/2}$	+0.58	$^4F_{7/2}$
(22 529)	4399(sh)	0.02	22 726							
	4398.2	0.07	22 730[h,i]	22 725	92.4	$^4F_{3/2}$	+7.18	$^4F_{5/2}$	+0.16	$^4F_{7/2}$
$^2G_{9/2}$	4108.2	0.29	24 335[h,i]	24 332	97.9	$^2G_{9/2}$	+1.42	$^4G_{11/2}$	+0.35	$^2K_{15/2}$
	4104.3	0.02	24 358							
(24 509)	4100.3	0.30	24 382[h,i]	24 384	96.9	$^2G_{9/2}$	+2.41	$^4G_{11/2}$	+0.37	$^2K_{15/2}$
	4096.5	0.02	24 404							
	4085.0	0.02	24 473	24 490	98.5	$^2G_{9/2}$	+0.79	$^4G_{11/2}$	+0.36	$^2K_{15/2}$
	4072.1	0.23	24 551	24 565	99.0	$^2G_{9/2}$	+0.33	$^4G_{11/2}$	+0.30	$^2K_{15/2}$
	4062.3	0.24	24 610							
	4056.3	0.16	24 646[h,i]	24 649	98.8	$^2G_{9/2}$	+0.48	$^2K_{15/2}$	+0.48	$^4G_{11/2}$
	4055.1	0.02	24 653							
$^4G_{11/2}$	3849.2	1.29	25 972[h]	26 128	98.1	$^4G_{11/2}$	+0.85	$^2K_{15/2}$	+0.82	$^4G_{9/2}$
	3843.6	0.06	26 010							
(26 305)	3812.7	0.03	26 221	26 196	98.2	$^4G_{11/2}$	+0.87	$^4G_{9/2}$	+0.65	$^2K_{15/2}$
	3810.9	0.02	26 233							
	3803.7	1.92	26 289[h,i]	26 295	96.3	$^4G_{11/2}$	+1.72	$^2K_{15/2}$	+1.56	$^4G_{9/2}$
	3802(sh)	0.15	26 294							
	3797.4	2.25	26 326[h,i]	26 324	94.0	$^4G_{11/2}$	+2.70	$^4G_{9/2}$	+1.98	$^2K_{15/2}$
	3795(sh)	0.18	26 343							
	3792.3	0.10	26 362							
	3786.8	1.20	26 400							
	3783.2	3.60	26 426[i]	26 429	93.5	$^4G_{11/2}$	+2.45	$^2K_{15/2}$	+1.89	$^4G_{9/2}$
	3781.0	2.14	26 441							
	3777.0	3.60	26 468[i]	26 461	94.3	$^4G_{11/2}$	+1.93	$^2K_{15/2}$	+1.66	$^4G_{5/2}$
	3774(sh)	1.90	26 490							
	3770.3	0.08	26 516							
	3765.0	0.04	26 553							

[a]Crystal contains 0.15 at. % Er, ($1.7\times10^{19}/cm^3$).
[b]Multiplet manifolds of Er^{3+} ($4f^{11}$); calculated centroids are listed in parenthesis in cm^{-1}.
[c]Wavelength (angstroms); sh denotes shoulder; b denotes broad.
[d]Intensity of axial spectrum (4 K) in absorbance/cm.
[e]Energy of observed levels in cm^{-1}.
[f]Calculated energy levels for Er^{3+} ions occupying a charge-compensated Sr^{2+} (M_2) site having C_s symmetry; crystal-field parameters are given in Table VI.
[g]Percent free-ion mixture of wave functions based on the C_s symmetry crystal-field parameters (B_{nm}) reported in Table VI.
[h]Hot bands found in absorption to this level at 70, 133, 165, and 260 cm^{-1}; levels within the ground-state manifold, $^4I_{15/2}$, corresponding to these hot bands have an uncertainty of $\pm3\ cm^{-1}$ due to the breadth and shape of the hot bands.
[i]Levels used in fitting analysis.

spectra with different decay times. It is not clear whether the different decay rates correspond to spectroscopically distinct sites.

The rapid decay of $^3H_4$ may be due to intraionic or interionic effects. The former is possible because unusually large phonon energies are available in the phosphate apatites, and the energy separation between $^3H_4$ and $^3H_5$ is smaller than that between $^1G_4$ and $^3F_2$, or that between $^1D_2$ and $^1G_4$. Despite the relatively low thulium concentration in the crystal, cross-relaxation may also be important, given the strong electronic transitions observed in Table I and Fig. 3 and the near resonance evident for the process

TABLE V. Emission from $^4S_{3/2}$ to $^4I_{15/2}$ at 4 K (Er:SFAP).[a]

λ(Å)[b]	$E(cm^{-1})$[c]	I[d]	Trans.[e]	$\Delta E(cm^{-1})$[f]	$E(cm^{-1})_{calc}$[g]
5477.5	18 251	vw			
5492.7	18 201	s	$B_1 \rightarrow Z_1$	0	−7
5502.1	18 170	vw			
5513.9	18 131	vs	$B_1 \rightarrow Z_2$	70[h]	65
5529.5(sh)	18 080	m			
5533.2	18 068	vs	$B_1 \rightarrow Z_3$	133[h]	136
5542.9	18 036	m	$B_1 \rightarrow Z_4$	165[h]	173
5556.1	17 993	m			
5572.2	17 941	m	$B_1 \rightarrow Z_5$	260[h]	260
5600(b)	17 853	w		348[i]	359
5638	17 731	vw		470[i]	478
5688.2	17 575	vw			
5709.9	17 509	vs	$B_1 \rightarrow Z_8$	692	694

[a]Excitation at 520 nm ($^2H_{11/2}$ multiplet manifold).
[b]Fluorescence measured in angstroms.
[c]Energy in vacuum wavenumbers.
[d]Relative intensity (see Fig. 11); vw (very weak); w (weak); m (medium); s (strong); vs (very strong).
[e]Transition from lowest energy Stark level of $^4S_{3/2}$ corresponding to 18 203 cm^{-1} in absorption (see Table III), to Stark levels of $^4I_{15/2}$ (Z_n).
[f]Difference in energy (cm^{-1}) using B_1=18201 cm^{-1}.
[g]Calculated splitting of the $^4I_{15/2}$ multiplet manifold using crystal-field parameters (B_{nm}) given in Table VI.
[h]Stark levels identified in absorption from hot bands are listed as Z_1=0, Z_2=70, Z_3=133, Z_4=165, and Z_5=260 cm^{-1}.
[i]Levels not used in fitting analysis.

($^3H_6$ lowest state, $^3H_4$ lowest state)→($^3F_4$ highest state, $^3F_4$ highest state).

Room temperature fluorescence branching ratios for $^1G_4$, Tm:SFAP, have been reported by Merkle, Zandi, and Chai.[29] For convenience we include their results here as follows ($^3H_6$, 0.80), ($^3F_4$, 0.10), ($^3H_5$, 0.05), ($^3H_4$, 0.05), and ($^3F_3$, $^3F_2$, < 0.1). We do not have branching ratios for other fluorescing manifolds.

V. CALCULATED CRYSTAL-FIELD SPLITTING FOR Tm:SFAP

The initial B_{nm} parameters used in the crystal-field splitting calculations were derived from a lattice-sum calculation in which trivalent thulium substitutes for divalent strontium in the M(II) site (C_s symmetry). The nearest-neighbor fluoride (F^-) is assumed to be replaced by divalent oxygen (O^{2-}) thus preserving overall charge neutrality and local symmetry.[18]

The total Hamiltonian for Tm^{3+} includes the free-ion coulombic and spin-orbit terms for all $SLJM_J$ states of the $4f^{12}$ electronic configuration and the crystal electric field terms reflecting C_s symmetry. The Racah and spin-orbit parameters entering into the free-ion part were obtained from an analysis of the aqueous solution spectra.[30] The crystal-field Hamiltonian is of the form

$$H_{\mathrm{CEF}} = \sum_{n\ \mathrm{even}} \times \sum_{m=-n}^{n} B_{nm}^{*} \sum_{i=1}^{12} C_{nm}(i), \tag{1}$$

where the B_{nm} are the crystal-field parameters, and the C_{nm} are expressed as

$$C_{nm}(i) = \left[\frac{4\pi}{(2n+1)}\right]^{1/2} Y_{nm}(\theta_i, \rho_i) \tag{2}$$

with

$$C_{n-m} = (-1)^m C_{nm}^{*}. \tag{3}$$

The Y_{nm} are spherical harmonics. In C_s symmetry values of m are restricted by $n + m = 0, \pm 2, \pm 4$, with $|m| \leqslant n$ and $n = 2,4,6$. The n-even B_{nm} parameters are restricted to 15 in C_s symmetry, but with a simple rotation about the principal

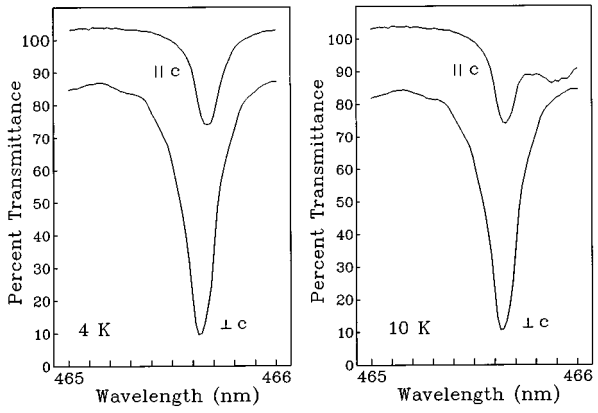

FIG. 4. Transverse absorption spectra of emitting level in $^1G_4$ (4757 Å, Table I at 4 K and 10 K showing the growth of a hot band that represents a transition from a Stark level 4 cm^{-1} above the ground-state Stark level.

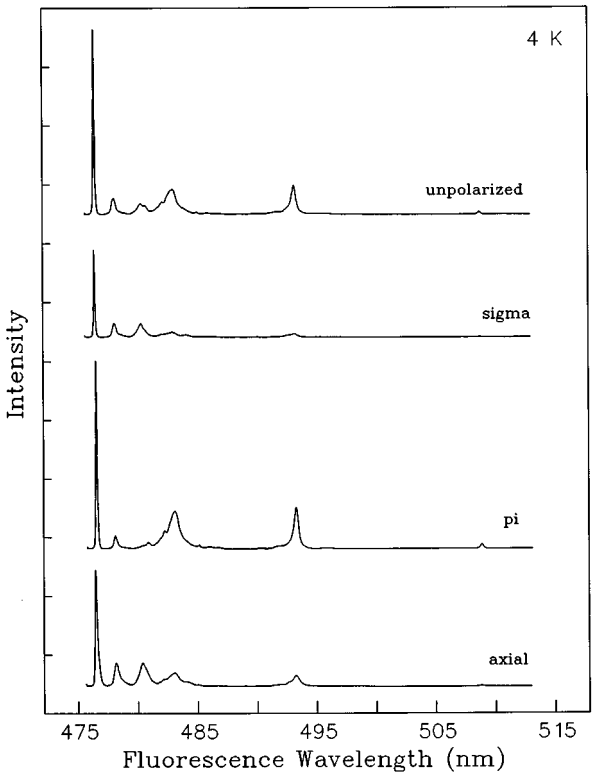

FIG. 5. Polarized emission spectra (transverse and axial) from the $^1G_4$ to the $^3H_6$ multiplet manifold at 4 K.

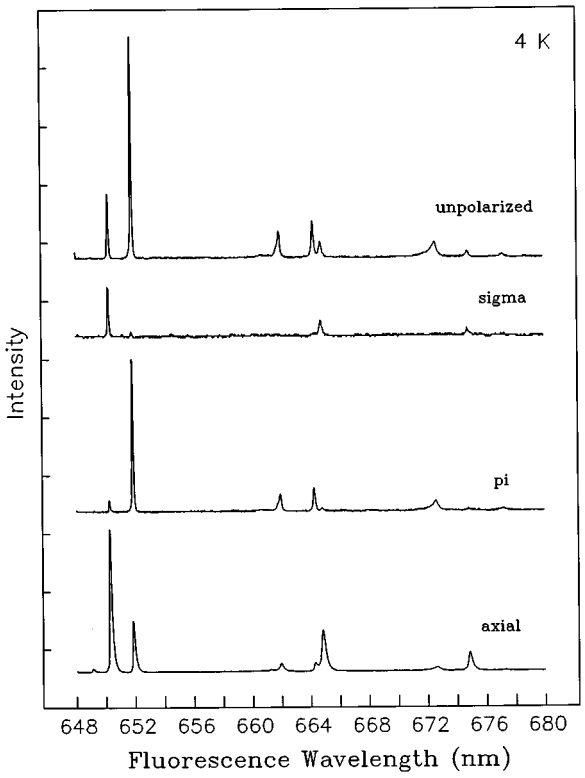

FIG. 6. Polarized emission spectra (transverse and axial) from the $^1G_4$ to the $^3F_4$ multiplet manifold at 4 K.

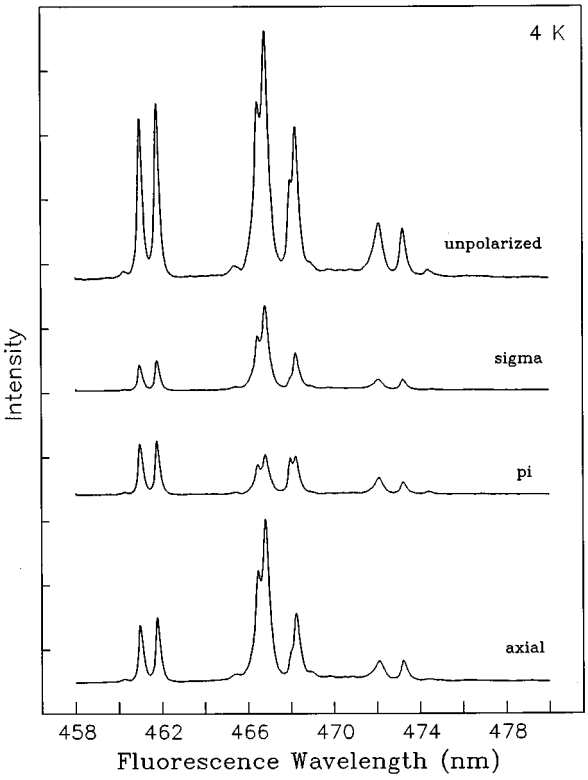

FIG. 8. Polarized emission spectra (transverse and axial) from the $^1D_2$ to the $^3F_4$ multiplet manifold at 4 K.

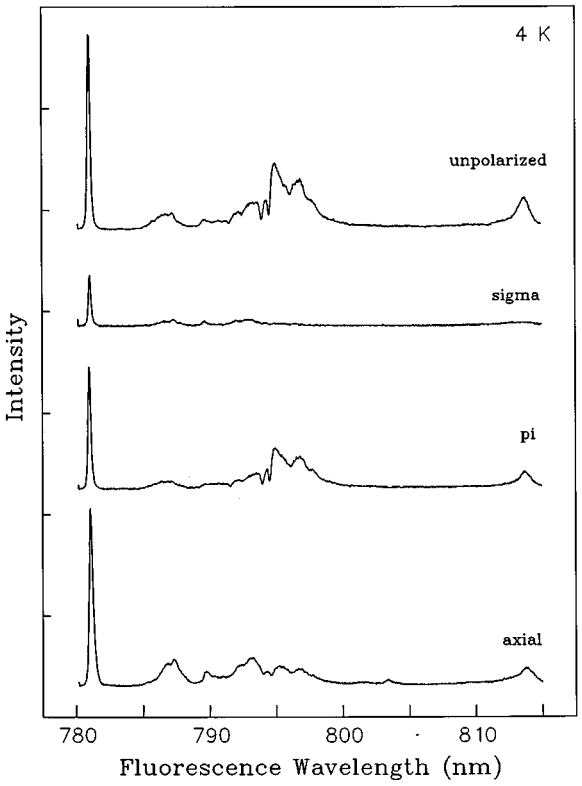

FIG. 7. Polarized emission spectra (transverse and axial) from the $^1G_4$ to the $^3H_5$ multiplet manifold at 4 K.

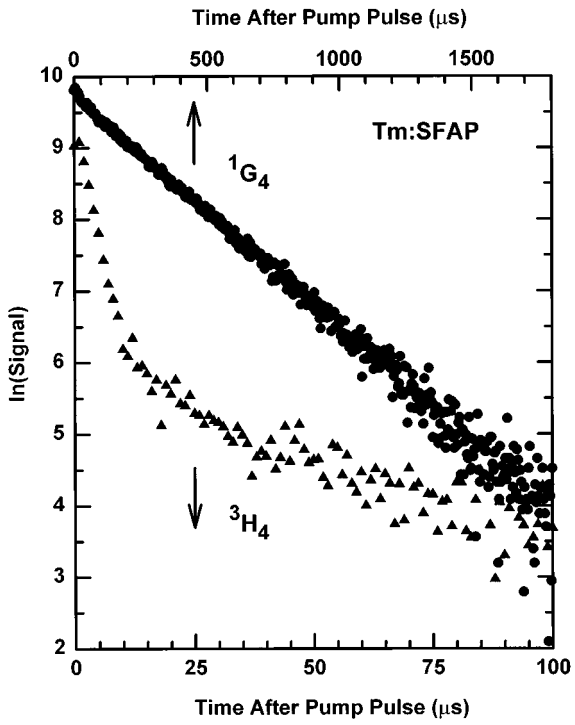

FIG. 9. Room temperature fluorescence decay waveforms for Tm:SFAP $^1G_4$ and $^3H_4$ fluorescence following pulsed excitation. The upper time scale applies to the $^1G_4$ decay, the lower scale to the $^3H_4$ decay.

TABLE VI. Crystal-field components and parameters for Tm^{3+} and Er^{3+} in SFAP (sites of C_s symmetry).[a]

A_{nm}	(cm^{-1}/Å^n)	B_{nm}	Tm^{3+} (cm^{-1}) final	Er^{3+} (cm^{-1}) predicted	Er^{3+} (cm^{-1}) final
A_{20}	11 057	B_{20}	2009	1886	1882
A_{22}	657	B_{22}	295	112	28.7
A_{40}	2053	B_{40}	876	1177	1462
Re A_{42}	455	Re B_{42}	204	188	261
IA_{42}	−1861	IB_{42}	− 934	− 768	−784
Re A_{44}	524	Re B_{44}	124	216	− 41.2
IA_{44}	764	IB_{44}	536	315	99.0
A_{60}	288	B_{60}	434	283	−158
Re A_{62}	−48	Re B_{62}	− 122	− 47	− 76.3
IA_{62}	−267	IB_{62}	− 26.8	− 262	−147
Re A_{64}	−289	Re B_{64}	− 185	− 284	−324
IA_{64}	38.0	IB_{64}	− 141	37.0	341
Re A_{66}	117	Re B_{66}	47.5	115	141
IA_{66}	−1147	IB_{66}	−1601	−1127	−438

[a]In the table ''Re'' denotes real and ''I'' denotes imaginary.

axis, B_{22} is made real and positive thus reducing the number of parameters to 14.[29] The B_{nm} are related to the crystal-field components, A_{nm}, by the expression,

$$B_{nm}=\rho_n A_{nm} \tag{4}$$

where

$$A_{nm}=-e^2\sum_j q_j C_{nm}(\hat{R}_j)/R_j^{n+1}. \tag{5}$$

In Eq. (4) ρ_n represents the effective value of $\langle r^n\rangle$ associated with the monopole A_{nm}. In Eq. (5) the effective charge is q_j on the ion at $\hat{R}_j$, and the sum is taken over all ions in the lattice.[31–33] The A_{nm} components were calculated for the M(II) site (C_s symmetry) using the x-ray data reported for SFAP.[18,22] The effect of replacing the nearest F^- site by an O^{2-} site was obtained by calculating the A_{nm} for a negative charge at this site and adding these components to the A_{nm} components for the M(II) site without charge compensation.[18] A value of $q=-2.00$ for the oxygen charge was chosen.

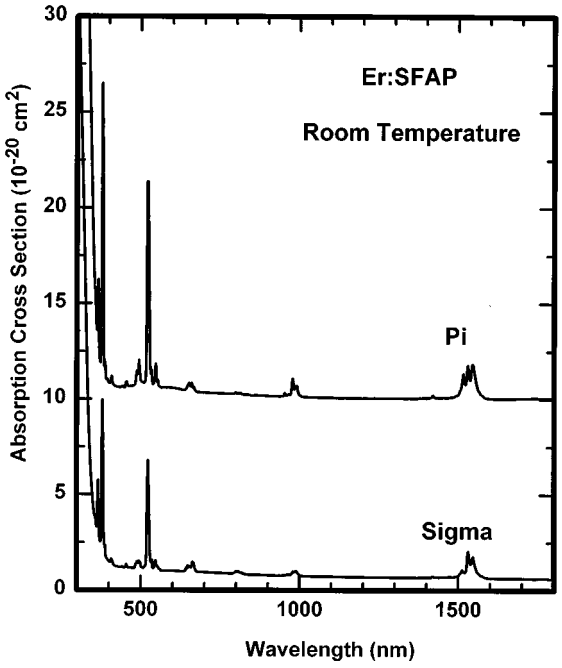

FIG. 10. Room temperature absorption spectrum of Er:SFAP.

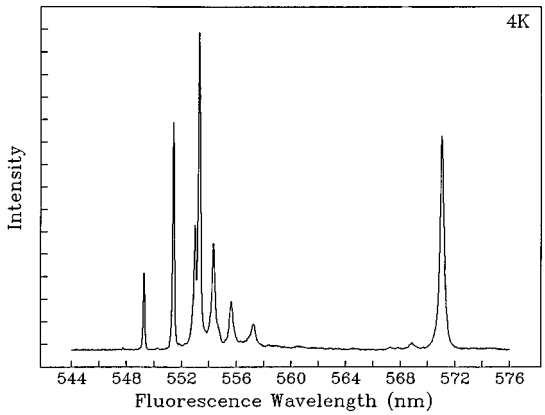

FIG. 11. Fluorescence from the $^4S_{3/2}$ to the $^4I_{15/2}$ multiplet manifold observed at 4 K.

Using the calculated B_{nm} parameters in the crystal-field splitting calculations, we obtained predicted Stark levels with symmetry labels that are consistent with conclusions obtained from experiment. The predicted ground-state Stark level and the first excited Stark level were several wavenumbers apart and of different symmetry (consistent with experimental results reported in Tables II and III. The splitting of the two lowest energy Stark levels in $^3H_5$ were also predicted to be of different symmetry and separated by several wavenumbers. The experimental assignments for these levels are 8209 (Γ_2) and 8212 cm^{-1} (Γ_1) in Table II and 8208 (Γ_2) and 8212 cm^{-1} (Γ_1) in Table III. These assignments are based on some of the strongest fluorescence observed. The predicted symmetry label for the emitting Stark level in the $^1D_2$ and $^1G_4$ manifolds give polarization patterns consistent with experiment.

Not all Stark levels of $^3H_6$ were observed. Because of the size of the crystal-field splitting, the J-mixing between multiplet manifolds $^3H_6$ and $^3F_4$ affects the splitting of the $^3F_4$ manifold. The 5677 cm^{-1} (Γ_1) Stark level in particular appears to be affected by Stark levels not identified in the $^3H_6$ manifold. While the predicted value for the 5677 cm^{-1} level is close to a weaker absorption peak observed at 5717 cm^{-1} in Table I, the latter does not appear in fluorescence. Consistent analysis of the fluorescence spectra matches the stronger absorption peak at 5677 cm^{-1} to a level observed in fluorescence.

Numerous least-squares fitting routines were used to maximize agreement between all experimental Stark levels identified from the polarized fluorescence spectra and calculated Stark levels whose energy as well as symmetry label most closely agree with experiment. The list of experimental levels was then expanded to include the most intense peaks observed in absorption. The best overall agreement obtained between calculated and experimental Stark levels is repre-

sented by the calculated splitting appearing in Tables I–III in which an rms deviation of 7 cm^{-1} was obtained between 43 calculated and observed levels. Because of the large crystal field, Table I also includes the percent of free-ion mixture. The final set of B_{nm} parameters for Tm^{3+} in Tm:SFAP is given in Table VI.

VI. ANALYSIS OF THE Er:SFAP SPECTRA AND FLUORESCENCE LIFETIME MEASUREMENTS

Table IV presents the absorption spectrum of Er:SFAP obtained at 4 K. A room temperature survey spectrum is given in Fig. 10. Both spectra are distinguished by having $J+1/2$ relatively strong absorption speaks associated with each multiplet manifold of $Er^{3+}(4f^{11})$. In addition to these strong peaks, much weaker and usually broad peaks, many appearing as satellite peaks to the strong peaks, are observed in the absorption spectrum and are attributable to Er^{3+} ions in minority sites in SFAP. The spectrum appearing in Table IV is much simpler than the absorption spectrum for Er^{3+} ions in Er:FAP reported by Gruber *et al.*[11] In C_s symmetry all Stark levels for Er^{3+} have the same symmetry label, $^2\Gamma_6$, and transitions in both σ- and π-polarization are allowed between these levels without restriction. The intensities of individual transitions appearing in the axial spectrum at 4 K are listed in Table IV (col. 3).

Fluorescence spectra from the $^4S_{3/2}$ multiplet manifold to the ground-state manifold, $^4I_{15/2}$, are reported in Table V and are displayed in Fig. 11. We were not able to completely reduce the emission to a single site, as a second site is apparent, having comparable splitting, as evidenced by a weaker emission spectrum that is nearly superimposed on the emission attributed to Er^{3+} ions in the majority site. Measurement of the temporal decay of the room temperature fluorescence from the $^4I_{11/2}$ and $^4I_{13/2}$ manifolds yields fluorescence lifetimes of 230 ± 20 μs and 8.9 ± 0.1 ms, respectively. These data are uncorrected for reabsorption effects, as reabsorption is considered to be minimal due to the dilution of the samples and the low absorption cross-sections. The lifetimes are somewhat shorter than were observed for erbium in FAP,[11] possibly indicating the presence of nonradiative relaxation channels in SFAP that are not present in FAP, though larger radiative transition probabilities may also contribute to the lifetime shortening.

Irradiation of the nominally 1% Er:SFAP sample with the 978 nm diode array at a fluence of greater than 1.2 kW/cm^2 produced no upconversion emission from the $^4S_{3/2}$ manifold, indicating that cross relaxation between ions excited into the $^4I_{11/2}$ manifold is not a dominant relaxation path.

The crystal-field splitting analysis of Er:SFAP was carried out by deriving a set of B_{nm} parameters for Er^{3+} ions from the final set of B_{nm} parameters obtained for Tm^{3+} that are listed in Table VI. The predicted set of B_{nm} parameters for Er^{3+} were calculated using the A_{nm} crystal-field components appearing in Table VI and the values of ρ_n obtained from Ref. 32. The Stark levels obtained from the $J+1/2$ strong absorption peaks associated with each multiplet manifold of Er^{3+} in Er:SFAP reported in Table IV were compared with the calculated levels using the predicted B_{nm} parameters for Er^{3+}. With modest change to most predicted B_{nm} parameters we were able to obtain a final rms deviation of 7 cm^{-1} between 43 experimental and calculated levels. The final set of B_{nm} parameters for Er^{3+} appears in column 6 of Table VI. Examination of the spectra reported in Table IV indicates that the $J+1/2$ absorption peaks used in our analysis represent more than 95% of the total absorption by all Er^{3+} ions in the crystal. The majority of Er^{3+} ions occupy a site of C_s symmetry. The free-ion mixture is also given in Table IV since the relatively large crystal-field splitting mixes states of adjacent manifolds to some extent, e.g., $^4F_{5/2}$ and $^4F_{3/2}$.

VII. CONCLUSIONS

From an analysis of the absorption and site-selective polarized fluorescence data, we conclude that the majority of Tm^{3+} and Er^{3+} ions occupy sites of C_s symmetry. Results support the conclusion that Tm^{3+} and Er^{3+} ions substitute for Sr^{2+} at the M(II) site in the undoped lattice. The nearest-neighbor fluoride (F^-) is replaced by divalent oxygen (O^{2-}) thus preserving overall charge neutrality and local C_s symmetry. The crystal-field splitting of individual multiplet manifolds represents some of the largest splittings observed for these ions in insulator host crystals. Consequently, J-mixing is relatively larger for certain manifolds (see for example, ^4F_J, Er:SFAP, Table IV). Larger J-mixing also affects the oscillator strengths that represent the intensities of the absorption and fluorescence spectra.

Absorption transitions from the ground-state to excited Stark levels within a given manifold exhibit a greater range of individual intensities than found for comparable transitions of the same ion in other low symmetry host crystals. For example, of the $J+1/2$ Stark level transitions allowed from the ground-state to the $^4I_{13/2}$ manifold in Er:SFAP, two of seven allowed transitions represent more than 90% of the absorption to this manifold at 4 K. Hot band absorption in both Tm:SFAP and Er:SFAP is very weak in comparison with the hot band absorption spectra observed in Tm:YAG[34] and Er:YAG.[35]

Due to the moderately long $^4I_{11/2}$ fluorescence lifetime in Er:SFAP, (230 ± 20 μs, room temperature) this material will probably not make a good host for Yb to Er-sensitized 1.5 μm laser action, as the energy transfer to the erbium from the ytterbium would be inefficient. Direct pumping into the $^4I_{13/2}$ manifold to obtain 1.5 μm laser action would be difficult, as most of the oscillator strength is concentrated between the lowest Stark levels of the two manifolds. The long $^4I_{11/2}$ lifetime, in conjunction with the uneven distribution of oscillator strength for transitions between the $^4I_{11/2}$ and $^4I_{13/2}$ manifolds, may prove to be sufficient for development of an efficient 2.8 μm laser source.[14]

The large oscillator strength of the transition from the ground Stark level in $^4I_{15/2}$ to the lowest Stark level within the $^4I_{13/2}$ manifold in Er:SFAP indicates that this material may function as a passive Q-switch for erbium glass lasers operating at 1.53 μm.[3,9] However, the long $^4I_{13/2}$ lifetime (8.9 ± 0.1 ms) means that the Q-switch would probably re-

main transparent, allowing free-running lasing to occur after the generation of the Q-switched pulse.

[1] J. B. Gruber, C. A. Morrison, M. D. Seltzer, A. O. Wright, M. P. Nadler, T. H. Allik, J. A. Hutchinson, and B. H. T. Chai, J. Appl. Phys. **79**, 1746 (1996).

[2] L. D. De Loach, S. A. Payne, L. L. Chase, L. K. Smith, W. L. Kway, and W. F. Krupke, IEEE J. Quantum Electron. **QE-29**, 1179 (1993).

[3] J. B. Gruber and M. D. Seltzer, *Modeling of Saturable Q-switch Absorbers*, in Proceedings of the IEEE/LEOS Eighth Annual Meeting, San Francisco, CA, 1995 (unpublished), p. 54.

[4] A. O. Wright, M. D. Seltzer, J. B. Gruber, B. Zandi, L. D. Merkle, and B. H. T. Chai, J. Phys. Chem. Solids **57**, 1337 (1996).

[5] J. B. Gruber, J. A. Hutchinson, D. C. Harris, M. D. Seltzer, T. H. Allik, C. A. Morrison, and M. P. Scripsick, *Materials Research Society Symposium Proceedings*, edited by B. H. T. Chai, S. A. Payne, T. Y. Fan, and T. H. Allik (Materials Research Society, Pittsburgh, PA, 1994), Vol. 329, p. 209.

[6] L. D. De Loach, S. A. Payne, W. L. Kway, J. B. Tassano, S. N. Dixit, and W. F. Krupke, J. Lumin. **62**, 85 (1994).

[7] B. H. T. Chai, *Novel Laser Sources and Applications*, edited by J. F. Becker, A. C. Tam, J. B. Gruber, and L. Lam (SPIE, Bellingham, WA, 1994), p. 5.

[8] A. O. Wright, M. D. Seltzer, J. B. Gruber, and B. H. T. Chai, J. Appl. Phys. **78**, 2456 (1995).

[9] T. H. Allik, J. B. Gruber, M. D. Seltzer, M. E. Hills, K. Spariosu, R. D. Stultz, M. Birnbaum, C. A. Morrison, B. H. T. Chai, J. A. Hutchinson, and L. D. Merkle, OSA Proceedings on Advanced Solid-State Lasers, edited by L. L. Chase and A. A. Pinto (Optical Society of America, Washington DC, 1993), Vol. 15, p. 246.

[10] P. Hong, X. X. Zhang, R. E. Peale, H. Weidner, M. Bass, and B. H. T. Chai, J. Appl. Phys. **77**, 294 (1995).

[11] J. B. Gruber, M. D. Seltzer, M. E. Hills, T. H. Allik, J. A. Hutchinson, C. A. Morrison, and B. H. T. Chai, Opt. Mater. **3**, 99 (1994).

[12] R. C. Ohlmann, K. B. Steinbruegge, and R. Mazelsky, Appl. Opt. **7**, 905 (1968).

[13] F. M. Ryan, R. W. Warren, R. H. Hopkins, and J. Murphy, J. Electrochem. Soc. Solid State Sci. **125**, 1493 (1978).

[14] J. B. Gruber, *Tunable Lasers for Engineering and Biological Applications* (SPIE, Bellingham, WA, 1992).

[15] G. V. Maksimova and A. A. Sobol', Inorg. Mater. **8**, 945 (1972).

[16] G. V. Maksimova and A. A. Sobol', Tr. Fiz. Inst. Akad. Nauk SSSR **60**, 55 (1972).

[17] G. V. Maksimova and A. A. Sobol', Proc. P. N. Lebedev Phys. Inst. **60**, 59 (1974).

[18] C. A. Morrison, Point-Charge Analysis of Symmetry-Preserving Charge Compensation and Vacacies in the Fluorapatites $Ca_5(PO_4)_3F$ and $Sr_5(PO_4)_3F$, Army Research Laboratory Report. ARL-TR-703, Adelphi, MD 20783, June, 1995.

[19] M. E. Fleet and Y. M. Pan, J. Solid State Chem. **112**, 78 (1994).

[20] St. Narcy-Szabo, Z. Kristallogr. **75**, 387 (1930).

[21] R. W. Wyckoff, Cryst. Struct. **3**, 228 (1965).

[22] J. M. Hughes, M. Cameron, and K. D. Crowley, Am. Mineral. **74**, 870 (1989).

[23] M. Greenblatt and J. H. Pifer, J. Chem. Phys. **66**, 559 (1977).

[24] W. W. Piper, L. C. Kravitz, and R. K. Swank, Phys. Rev. A **138**, 1802 (1965).

[25] H. A. Bethe, Ann. Phys. (Leipzig) **3**, 133 (1929).

[26] J. L. Prather, Atomic Energy Levels in Crystals, NBS Monograph 19 (U.S. Department of Commerce, National Bureau of Standards, Washington D.C., 1961).

[27] C. Li, A. Lagriffoul, R. Moncorgé, J. C. Souriau, C. Borel, and Ch. Wyon, J. Lumin. **62**, 157 (1994).

[28] G. H. Rosenblatt, G. J. Quarles, L. Esterowitz, M. Randles, J. Creamer, and R. Belt, Opt. Lett. **18**, 1523 (1993).

[29] L. D. Merkle, B. Zandi, and B. H. T. Chai, *Spectroscopic Evaluation of the Visible Laser Potential of Several* Pr^{3+} *and* Tm^{3+} *Doped Crystals*, OSA Trends in Optics and Photonics on Advanced Solid State Lasers, edited by S. A. Payne and C. R. Pollack (Optical Society of America, Washington, DC, 1996), Vol. 1, pp. 516–521.

[30] W. T. Carnall, P. R. Fields, and K. Rajnak, J. Chem. Phys. **49**, 4412 (1968); **49**, 4424 (1968); **49**, 4443 (1968); **49**, 4450 (1968).

[31] C. A. Morrison and R. P. Leavitt, J. Chem. Phys. **71**, 2366 (1979).

[32] C. A. Morrison, *Angular Momentum Theory Applied to Interactions in Solids*, Lecture Notes in Chemistry (Springer-Verlag, New York, 1988), Vol. 47.

[33] C. A. Morrison, *Crystal Fields for Transition-Metal Ions in Laser Host Materials* (Springer-Verlag, New York, 1992).

[34] J. B. Gruber, M. E. Hills, R. M. Macfarlane, C. A. Morrison, G. A. Turner, G. J. Quarles, G. J. Kintz, and L. Esterowitz, Phys. Rev. B **40**, 9464 (1989).

[35] J. B. Gruber, J. R. Quagliano, M. F. Reid, F. S. Richardson, M. E. Hills, M. D. Seltzer, S. B. Stevens, C. A. Morrison, and T. H. Allik, Phys. Rev. B **48**, 15–56 (1993).